Extensive eigenchannel R-matrix study of the H^- photodetachment spectrum

H. R. Sadeghpour
Harvard-Smithsonian Center for Astrophysics, 60 Garden Street, Cambridge, Massachusetts 02138

Chris H. Greene
Department of Physics, University of Colorado, Boulder, Colorado 80309-0440
and Joint Institute for Laboratory Astrophysics, University of Colorado, Boulder, Colorado 80309-0440

Michael Cavagnero
Department of Physics and Astronomy, The University of Kentucky, Lexington, Kentucky 40506-0055
(Received 2 August 1991)

We combine an eigenchannel R-matrix calculation with an analytic description of electron motion in a dipole field to predict photodetachment cross sections of the hydrogen negative ion, including resonant structures up to the $n=4$ hydrogenic threshold. Partial cross sections for the production of hydrogen-atom fragments in states with specific principal quantum numbers n are also presented for comparison with a recent experiment. An analysis of the delay-time matrix indicates that the autodetaching Feshbach resonances decay primarily into the nearest energetically accessible continuum channel, an observation which is not at all apparent from the calculated and observed partial cross sections, but has been anticipated in previous theoretical work. We find, for instance, that the ${}_{n=4}\{v=0\}_{m=4}^{A=+}$ resonant state below the $H(n=4)$ threshold decays 73% of the time to the ${}_3\{0\}^+$ photodetachment channel.

PACS number(s): 31.50.+w, 32.80.Dz, 32.80.Fb, 82.50.Fv

I. INTRODUCTION

The spectroscopy of the hydrogen negative ion remains at the forefront of investigations of correlated electron motion. The spectrum of H^- is simple in that it has only one bound state, and in that the nature of its continua is governed, in a large part, by the long-range interaction of one electron with the induced "permanent" dipole of a neutral hydrogen "core." The permanent dipole results from the mixing of degenerate orbital angular momentum states of the excited H atom by the field of the distant electron, and the field of this dipole can in turn either repel or resonantly bind that electron. Despite the overall simplicity of this spectrum, experimental investigations continue to reveal a rich dynamics which has yet to be fully incorporated in theory.

Doubly excited states of H^- have been observed primarily by Bryant and co-workers using the Los Alamos Meson Physics Facility (LAMPF) relativistic ion beam. Since the later 1970s, Bryant and co-workers [1,2] have excited H^- ions with high-energy photons using a technique based on the relativistic Doppler effect. The group has recently observed resonant states of H^- which autodetach to $H(n)+e^-$ continua with principal quantum numbers up to and including $n=8$ [3,4]. By measuring partial cross sections for the production of H-atom fragments in particular n-manifolds, they have identified the dominant photodetachment channels. Their results have been interpreted qualitatively [5], but they have not yet been reproduced in quantitative calculations.

Existing theory of H^- photodetachment is multifaceted. Regularities of resonant structures have been uncovered and organized in group-theoretic classification schemes [6–8], the hyperspherical adiabatic representation [9–12], and molecular-orbital (MO) models [13,14]. These studies reveal approximate symmetries of the two-electron Hamiltonian, and serve to classify resonances according to "radial" and "angular" correlation patterns. While these approaches provide considerable insight into experimentally observed regularities, they cannot provide quantitative comparison with experimental cross sections. Other methods have aimed at providing accurate resonance energies and lifetimes, principally the complex rotation method [15,16] and the variationally adjusted multiconfiguration Hartree-Fock approach [17].

Actual *ab initio* calculations of the photodetachment cross sections are comparatively few [18–21], and no theoretical calculation has yet been presented that includes resonance near the $H(n=4)$ threshold. Aside from Broad and Reinhardt's original work [18] on the ${}^1P^o(n=2)$ shape resonance and the lowest ${}^1P^o(n=2)$ Feshbach resonance, attempts to calculate the cross sections have been limited to the R-matrix method. The enormous size of the high-lying resonances, which grow in proportion to n^2, and the need to incorporate the dipole character of the detachment channels complicate this application. In this paper, we report results obtained using the eigenchannel form of the R-matrix theory.

We present detailed results of an eigenchannel R-matrix calculation of the photodetachment cross sections of H^- in the vicinity of the $n=2$, 3, and 4 thresholds. Our results verify that the spectrum in the vicinity of each hydrogenic threshold is dominated by a single ridge-riding resonance in which the two electrons are in nearly equal radial orbits from the proton [22]. We also

present partial cross sections for comparison with experimental work. We find that dominant decay modes of the individual resonances cannot in all cases be determined from the partial cross sections. An analysis of the eigenvectors of the delay-time matrix [23] indicates that each observed resonance decays primarily to the nearest energetically accessible continuum with similar angular and radial correlation.

The observed resonances have been classified [5,24,25] according to the scheme ${}_n\{v\}_m^A$, where the vibrational quantum number $v=\frac{1}{2}(n-K-T-1)$ is related to Herrick's K and T correlation numbers [6,7]. The symbol $A=+$ $(-)$ specifies [26] that the two-electron wave function has an antinode (node) in the radial degree of freedom near the line $r_1=r_2$. This quantum number was first introduced by Cooper, Fano, and Pratts [27]. The label m denotes the degree of radial excitation of the outer electron [24].

II. NUMERICAL PROCEDURE

The eigenchannel R-matrix method has been used extensive to describe photoabsorption spectra of atoms with two valence electrons, namely the alkaline-earth-metal [28–30] and the alkali-metal negative ions [31]. Adaptation of this method to treat H^- photodetachment in LS coupling follows these earlier studies to a large extent. The "accidental degeneracy" of H^- photodetachment thresholds is, however, peculiar to this system, requiring the incorporation of a long-range dipole interaction between the outgoing electron and the excited hydrogen fragment.

A. The eigenchannel R matrix

This method aims to determine variationally a set of normal logarithmic derivatives $-b_\beta$, amounting to eigenvalues of the Wigner R matrix, which are constant across a reaction surface S enclosing a reaction volume V. The reaction volume is usually intended to contain the entire region of configuration space over which the interacting particles can exchange energy. For the two-electron systems treated along the lines of Refs. [29–31], the reaction volume V is the portion of the six-dimensional configuration space $(\mathbf{r}_1,\mathbf{r}_2)$ for which both electrons lie within a sphere of radius r_0. The reaction surface S is the set of points for which $\max\{r_1,r_2\}=r_0$. In practice, for any given energy range of interest, the radius r_0 is taken to be sufficiently large such that the probability of both electrons escaping simultaneously beyond r_0 can be neglected. The complicated dynamics of the two interacting electrons inside the reaction volume is then represented by a variationally optimized superposition of many LS-coupled independent-electron basis functions.

In applications to date [29–31], the long-range multipole interactions between the electrons were sufficiently weak outside the R-matrix box to permit neglect of *angular momentum exchange* (as well as energy exchange) at $r>r_0$. The main difference between H^- photodetachment process producing excited hydrogen atoms $H(nl_1)$ and the systems treated in Refs. [29–31] is the degeneracy of the n atomic energy levels E_{nl_1} having $l_1=0,\ldots,n-1$. This degeneracy leads to angular momentum exchange between the H^- electrons even out to extremely large distances $r\gg r_0$, an effect which can be described using the "dipole representation" of Seaton [32] and of Gailitis and Damburg [33]. The effect of an escaping electron on this degenerate hydrogenic manifold is to superpose spherical channel functions (labeled by $i=\{n,l_1,l_2\}$) by an orthogonal transformation X_{ij}, thus producing a permanent dipole moment a_j in the hydrogen atom. The interaction of this dipole with the escaping electron at $r_2>r_0$ is represented by an effective potential

$$V(r_2)\rightarrow\frac{a_j}{2r_2^2}\ . \tag{1}$$

Note that j denotes a pair of quantum numbers $j=\{n,\mu\}$, where μ is a label distinguishing available dipole channels within the n manifold.

The channel dipole moments a_j and the real orthogonal transformation matrix X_{ij} connecting dipolar channels and ordinary spherical channels $i\equiv\{n,l_1,l_2\}$ for a given L, S, and parity π are obtained using degenerate perturbation theory [32,33]. Specifically, one collects all terms in the large-r_2 close-coupling equations which are of order $1/r_2^2$. Assuming r_2 is much larger than the inner electron radius r_1, we neglect exchange terms outside the box which are decaying exponentially; the resulting interaction potential matrix connecting degenerate spherical channels then takes the form (in a.u.)

$$\frac{1}{2r_2^2}\langle\Phi_i|l_2^2+2\mathbf{r}_1\cdot\hat{\mathbf{r}}_2|\Phi_{i'}\rangle\equiv\frac{1}{2r_2^2}A_{ii'}\ . \tag{2}$$

The matrix element in (2) is a five-dimensional integral over $(\mathbf{r}_1,\hat{\mathbf{r}}_2)$, where the spherical channel function is

$$\Phi_i(\mathbf{r}_1,\hat{\mathbf{r}}_2)=R_{nl_{1i}}(r_1)Y_{l_{1i}l_{2i}LM}(\hat{\mathbf{r}}_1,\hat{\mathbf{r}}_2)\ . \tag{3}$$

The most important couplings in Eq. (2) are those connecting degenerate channels, i.e., those having the same n. Accordingly we neglect the matrix elements coupling nondegenerate channels, and diagonalize the resulting real, symmetric matrix $A_{ii'}$. The eigenvalues of this matrix are the desired channel dipole moments a_j, and the corresponding eigenvectors constitute the orthogonal transformation matrix X_{ij}. Note that the neglected off-diagonal (in n) elements give rise to relatively short-ranged multipole potentials decaying faster than r_2^{-2} at $r_2\rightarrow\infty$. These, along with the exchange interaction, are neglected outside the R-matrix box, a practical constraint which determines the minimum acceptable size of the interaction volume V.

The dipole representation thus obtained defines a new set of channel functions ϕ_j, each of which is a linear combination of spherical channel function within the n manifold:

$$\phi_j=\sum_{l_{1i},l_{2i}}\Phi_iX_{ij}\ . \tag{4}$$

In the spirit of multichannel quantum-defect theory (MQDT) [34,35] the asymptotic form of the βth independent solution to the time-independent Schrödinger equation at any given energy E can be written as a dipole channel expansion at $r_2 > r_0$,

$$\Psi_\beta = \mathcal{A} r_2^{-1} \sum_j \phi_j(\mathbf{r}_1, \hat{\mathbf{r}}_2) F_{j\beta}(r_2) \ . \tag{5}$$

Here $\mathcal{A}$ denotes an antisymmetrization operator. Neglect of long-range multipole effects, except for the dipole interactions among degenerate channels, implies that each of the radial wave functions $F_{j\beta}(r_2)$ obeys the simple equation

$$\left[-\frac{1}{2}\frac{d^2}{dr_2^2} + \frac{a_j}{2r_2^2} - \varepsilon_j \right] F_{j\beta}(r_2) = 0 \ . \tag{6}$$

Here $\varepsilon_j = E + 1/2n^2$ is the asymptotic photoelectron energy in channel j in the hydrogenic manifold n. Note that some of the channels included at any energy are closed channels having $\varepsilon_j < 0$; for these channels the wave function in Eq. (5) diverges asymptotically as $r_2 \to \infty$. The application of the physical boundary conditions, i.e., the quantization of the wave function in Eq. (5), is done with the aid of quantum-defect methods.

Two independent solutions of the radial equation (6) can be denoted (f_j, g_j). These are functions of the Bessel class and are given explicitly elsewhere [36]. It is important to remember that these solutions are qualitatively different, depending on the sign of $a_j + \frac{1}{4}$. When this quantity is positive, channel j is said to have a repulsive dipole moment such that the dipole potential cannot by itself bind the outermost electron. When it is negative, channel j has an attractive dipole moment and the dipole potential in (6) supports an infinite number of quasibound states converging exponentially to the threshold energy $-1/2n^2$. Equation (6) implies that the large-r_2 form of the βth independent solution is

$$\Psi_\beta = \mathcal{A} r_2^{-1} \sum_j \phi_j(\mathbf{r}_1, \hat{\mathbf{r}}_2)[f_j(r_2) I_{j\beta} - g_j(r_2) J_{j\beta}] \ , \quad r_2 > r_0 \ . \tag{7}$$

The energy-dependent matrices $I_{j\beta}$ and $J_{j\beta}$ are determined by matching the variational R-matrix solution to the form (7) at $r_2 = r_0$. From these a dipole representation reaction matrix $K_{jj'} = \sum_\beta J_{j\beta}(I^{-1})_{\beta j'}$ is constructed. [In the present paper the base pair (f_j, g_j) is taken to be the *energy-normalized* solutions of Ref. [31]. Substantially smoother energy-dependent reaction matrices are obtained using radial functions which are *analytic in energy*, but since our main goal is to specify the photodetachment dynamics we will not make use of them in the following.] Standard references [34,35,37] describe how the reaction matrix and a set of dipole matrix elements d_β are used to evaluate observable quantities in the photodetachment process.

B. The delay-time matrix

Smith [23] has shown that a natural way of calculating the lifetime and decay modes, for a quasistable compound state formed as an intermediate state in a collision process, utilizes the lifetime of delay-time matrix

$$\underline{Q}(E) = -i\underline{S}^\dagger \frac{d\underline{S}}{dE} \ , \tag{8}$$

where $\underline{S}$ is the short-range unitary scattering unitary scattering matrix and $-i(d/dE)$ is the quantum time operator. For single-channel elastic-scattering processes, the quantity $Q(E)$ expresses the ratio of the excess number of electrons in the reaction zone to the out-going flux. The delay-time matrix constructed in this fashion is Hermitian and its largest eigenvalue $q_{\max}(E)$ can be identified with the decay time of a resonant state. The absolute squares of components of the eigenvector corresponding to $q_{\max}$ represent the probabilities for the quasistable state to decay into different available continua.

Components of the scattering matrix in the dipole representation are given in the language of MQDT (see Eqs. 17–20 in Ref. [34]) as

$$S_{jj'}(E) = \sum_{\rho=1}^{N_o} T_{j\rho} e^{2\pi i \tau_\rho} T_{j'\rho} \ , \tag{9}$$

where τ_ρ are the collision eigenphase shifts common to all fragmentation (detachment) channels j. $T_{j\rho}$ are the collision eigenvectors which form a real orthogonal matrix and N_o is the number of energetically accessible open channels.

The energy profile of the largest eigenvalue of the delay-time matrix is Lorentzian (Breit-Wigner) given by [23]

$$q_{\max}(E) = \frac{\Gamma}{(E - E_0)^2 + (\Gamma/2)^2} \ , \tag{10}$$

with E_0 the resonance energy having a full spread of Γ at half maximum.

III. RESULTS AND DISCUSSIONS

A. Classification scheme

To aid with the classification of the resonances in the photodetachment spectra (see below) and with the determination of the R-matrix reaction box size, we display in Fig. 1 the diabatic hyperspherical potential curves up to the H($n = 4$) threshold [5,9,24]. Only a select number of the $^1P^\circ$ diabatic potential curves are shown. The crossings of the diabatic curves between the $A = +$ and $-$ channels, first recognized by Macek [9] and Lin [10], indicate the minimal coupling between such curves. In the lowest state (labeled by $m = n$) in the $A = +$ potential-energy curve, the two electrons spend considerable time at comparable distances from the nucleus—they interact strongly via a repulsive Coulomb interaction—and are accordingly quite unstable, autoionizing rapidly. These comparatively broad resonances form a ridge series converging to the double continuum threshold [38]. Higher-lying energy levels in these channels (labeled by $m = n+1, n+2, \ldots \infty$) form dipole series converging to different n hydrogenic thresholds. In contrast, one electron typically roams far from the excited H atom in the

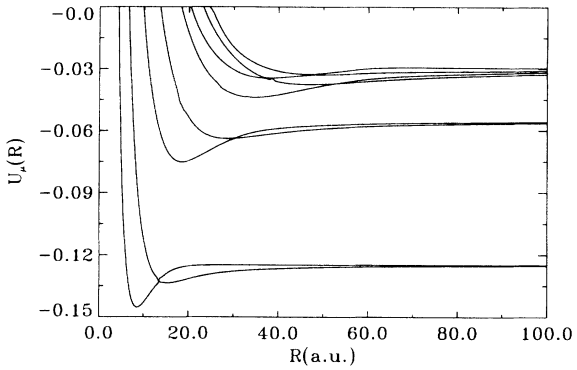

FIG. 1. Diabatic $^1P^\circ$ hyperspherical potential curves for the single-photon detachment of H^-. Only the "+" and "−" channels are shown. The asymptotic (large R) identification of these curves is according to the sequence ${}_n\{v\}^A = {}_n\{0\}^-$, ${}_n\{0\}^+, {}_n\{1\}^-, {}_n\{1\}^+, \ldots$.

$A = -$ resonances, interacting only weakly with it—predominantly through the long-range dipole potential. This relatively weak interaction enhances the stability of the resonance against autoionization. Of the possible $A = -$ channels, those with the largest dipole moments have the strongest interaction with the core and are accordingly most unstable producing visible resonant structure. For these strongly attractive dipole channels, infinite series of narrow resonances are labeled by $m = n+1, n+2, \ldots, \infty$. Roughly speaking, n and m can be viewed as principal quantum numbers of the inner and outer electrons, respectively.

All the resonance observed in H^- photodetachment to data can be classified as having $v = 0$ quantum number (described in Sec. I), meaning that they have only zero point motion in the "bending" coordinate $\theta_{12} = \cos^{-1}(\hat{\mathbf{r}}_1 \cdot \hat{\mathbf{r}}_2)$. This propensity for pure radial excitation was recently emphasized in a hyperspherical coordinate interpretation of the LAMPF spectra [5]. This quantum number and its alternative form as the number of nodes n_λ in the elliptical angular coordinate in the MO picture of Briggs and co-workers [13,14] takes on values of $0, 1, 2, \ldots$ for consecutive "+" or "−" channels in each hydrogenic n manifold. Hereafter, we use the notation ${}_n\{v\}^A_m$ used in Ref. [24] to label the resonances. The Gailitis-Damburg channel indices of Sec. II can also be approximately identified with $j \equiv {}_n\{v\}^A$, since each hyperspherical channel evolves adiabatically into a dipole channel as $R \to \infty$ [39].

B. Computational details

The results of this work stem from three separate calculations appropriate to each hydrogenic threshold region. Calculations near the $n = 2$ threshold were performed with a reaction box size of $r_0 = 25$ a.u. (The size of the R-matrix matching radius is chosen for the $^1P^\circ$ final-state channels somewhere beyond the diabatic crossing of + and − channels for each n of interest.) The total number of "closed" two-electron configurations (those configurations whose amplitudes vanish on the surface $r = r_0$) was 158 and 250 in the initial and final states, respectively. With 158 initial state configurations retained inside the R-matrix box, the ground-state energy of H^- was computed to be -0.52403 a.u., a value about 100 meV too high. In this region, there are four relevant photodetachment channels ($N_o = 4$, one for $n = 1$ three for $n = 2$). Two "open-type" orbitals were included in each of these four channels to represent the escape of photoelectrons [30,31].

For calculations near the $n = 3$ threshold, the box size was increased to $r_0 = 35$ a.u. The number of basis function was likewise increased to 300 and 514 closed configurations in initial and final states, respectively. As demonstrated below, this was sufficient to obtain agreement between length and velocity forms of the total photodetachment cross section. Two open-type orbitals for each of the nine accessible channels were also included.

Near the $n = 4$ threshold, a 16-channel MQDT calculation with a box size of $r_0 = 65$ a.u. was needed. A total of 372 and 646 configurations were retained in the initial and the final state, respectively. With this box size and basis set, total cross sections calculated in length and velocity form are spread by roughly 30%, though the shape of resonance features appears to be similar in the two calculations. Pilot calculations with smaller box sizes $r_0 \sim 30$ a.u. suggest that the velocity form is reasonably converged. (Length and velocity forms in these calculations agree to within 2%.)

We now turn our attention to giving the details of the resonance structures and their interpretation.

C. Partial and total cross sections

Our calculated total photoabsorption cross section of H^- (velocity form), spanning the $n = 2$, 3, and 4 thresholds of the hydrogen atom fragment, is shown in Fig. 2. A nonlinear energy scale has been used to separate the $-1/2n^2$ threshold by integer quanta. Note that Fig. 2 displays the results of three separate calculations

The total photoabsorption cross sections near the $n = 2$, 3, and 4 thresholds are presented in Figs. 3(a)–3(c), respectively. Both length and velocity forms are given,

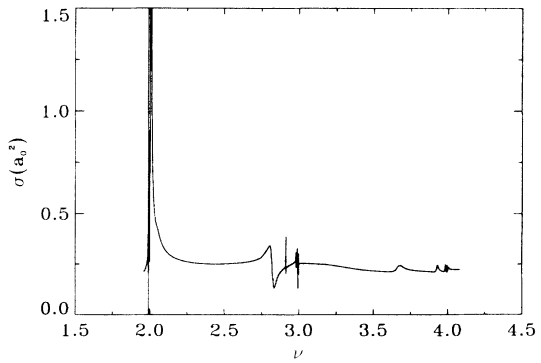

FIG. 2. Total resonant cross section of the excitation of the doubly excited states of H^- converging on the hydrogenic thresholds, at integer values of $\nu = (-2E)^{-1/2}$ at 2, 3, and 4. The height of the Feshbach and the shape resonances near $\nu = 2$ has been clipped.

except for the $n=2$ spectrum [Fig. 3(a)] where they are indistinguishable on the scale shown.

Focusing on the region of the $n=2$ threshold, Fig. 3(a), three resonances are apparent, labeled, respectively, ${}_2\{0\}_3^-$, ${}_2\{0\}_4^-$, and ${}_2\{0\}_2^+$. The two $A=-$ resonances are sequential members ($m=3,4$) of an infinite series of dipole resonances converging exponentially [see Eqs. (11) below] to the $n=2$ threshold. There is also a single broad shape resonance lying above the threshold. These $n=2$ resonance features have been the focus of a number of studies [10,18,20(b),20(c)], notable among which is the calculation of Broad and Reinhardt [18], which gave early and excellent agreement with experiment. Here, we simply note that our calculation confirms the Broad-Reinhardt result that the height of the narrow ${}_2\{0\}_3^-$ resonance (we obtain $\approx 95a_0^2$) is much higher than the height of the shape resonance.

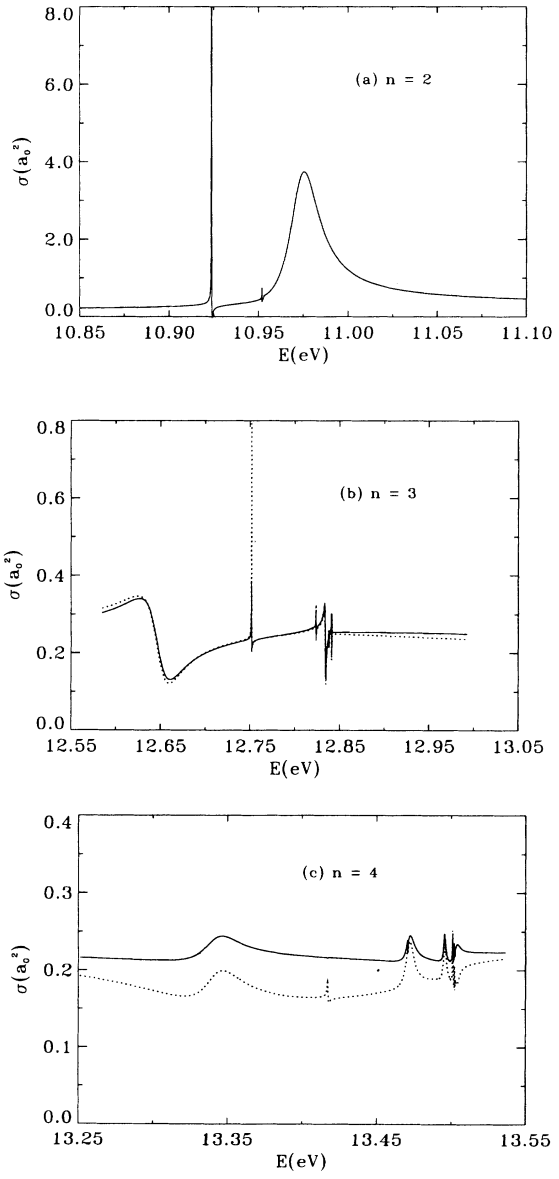

FIG. 3. Total cross sections near (a) the H($n=2$) threshold at 10.9530 eV, (b) the H($n=3$) threshold at 12.8417 eV, and (c) the H($n=4$) threshold at 13.5027 eV. The dotted lines are the length form cross sections and the solid lines give the velocity forms.

In Table I, the position and width of these states are tabulated along with the value of the dipole moments a_j for the respective Gailitis-Damburg channels $j={}_n\{0\}^A$. Comparison is also made with other calculations. The energies and width of the dipole members of the ${}_n\{0\}^+$ and ${}_n\{0\}^-$ series are well approximated by the dipole formula [33]

$$\frac{\varepsilon_{m+1}}{\varepsilon_m}=\frac{\Gamma_{m+1}}{\Gamma_m}=e^{-2\pi/\alpha_j}, \tag{11a}$$

where α_j is related to a particular dipole moment by

$$\alpha_j\equiv\sqrt{-a_j-\tfrac{1}{4}}\,. \tag{11b}$$

Resonant structure in the vicinity of the $n=3$ threshold, Fig. 3(b), already shows the appearance of two distinct series, labeled ${}_3\{0\}_{3,4,5}^+$ and ${}_3\{0\}_{4,5,6}^-$. Note that the two lowest member of the $-$ series lie between the two lowest members of the $+$ series. A larger effective dipole moment associated with the channel results in slower convergence of the series to threshold, in accordance with Eqs. (11). Our results are compared with the experimental spectrum of Bryant and co-workers [20] in Fig. 4. The narrow resonance have not yet been experimentally resolved, but agreement with the dominant $+$ resonance is excellent.

The total cross section near the H($n=4$) threshold, shown in Fig. 3(c), is once again dominated by a single series of resonances lying in the ${}_4\{0\}^+$ channel. Note that narrow $-$ resonances are seen in the length form of the cross section (which weights large distances), but are not quite visible in the velocity form (which we believe to be better converged). The position and width of the first member of the series, the ${}_4\{0\}_4^+$ Feshbach resonance, in Table I, compete quite favorably with values from other calculations, and are in substantial agreement with the recent observation of this resonance [40]. Note that this resonance and the ${}_3\{0\}_3^+$ resonance have opposite asymmetries. To interpret this and other features of the total

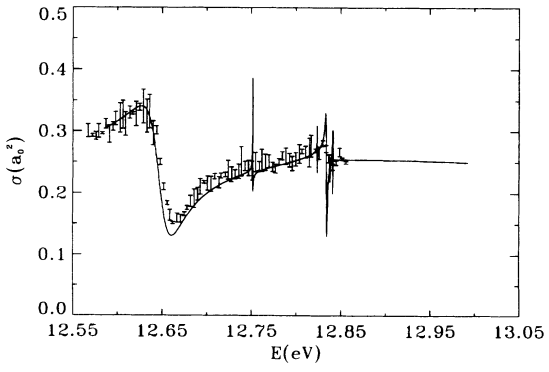

FIG. 4. Comparison of the total cross section spectrum of Ref. [2] with the present calculation. The broad ridge resonance ${}_3\{0\}_3^+$ is almost entirely reproduced.

cross sections, we turn now to an analysis of the partial cross sections and the delay-time matrix.

Figure 5(a) displays partial cross sections (velocity form) for the production of H atoms in either the $n=1$ or 2 states, for photon energies near the $n=2$ threshold. Below threshold, of course, only the $n=1$ state can be produced. However, the strong ${}_2\{0\}_2^+$ shape resonance can decay to either threshold. The figure clearly indicates that substantial production of ground-state atoms is limited to a range of roughly 0.03 eV above threshold. The ${}_2\{0\}_2^+$ shape resonance, which has a repulsive dipole interaction at large distances, decays principally by tunneling through the dipole barrier, producing $n=2$ H-atom fragments. (The height of the barrier calculated in an adiabatic hyperspherical approach [10] is ≈ 65 meV above the threshold.) Note that the tail of the resonance

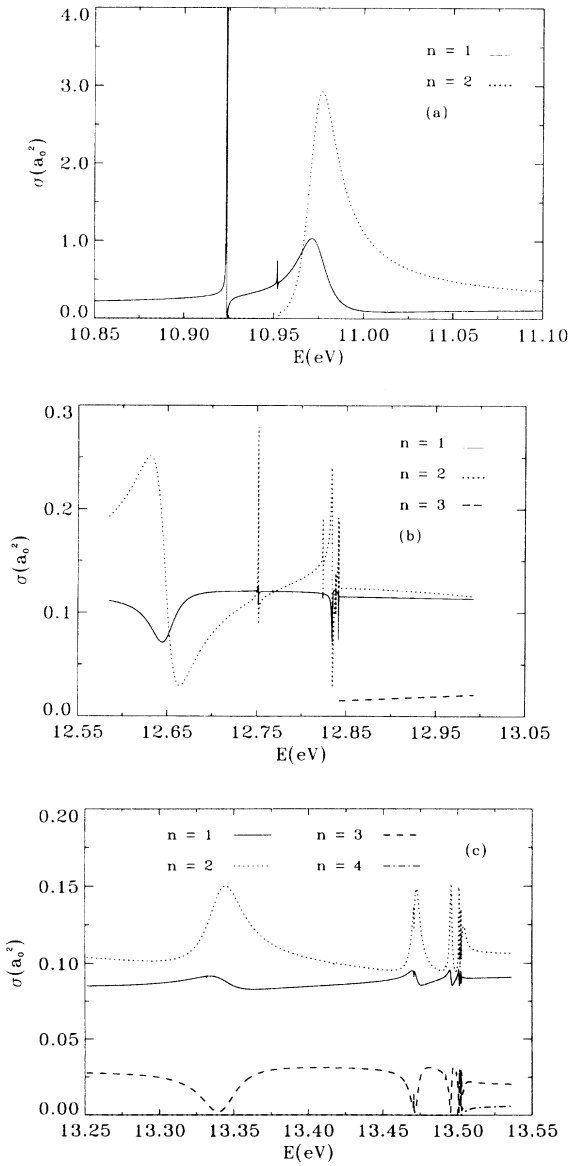

FIG. 5. The partial cross section for the production of individual states of hydrogen n at energies near (a) the $n=2$ threshold, (b) the $n=3$ excited state of hydrogen, and (c) the $n=4$ excited state.

TABLE I. Energies (E) relative to the double-escape threshold, widths (Γ), and Gailitis-Damburg Eigenvalues (a_j) in a.u. for the ${}^1P^o$ resonances in H^-

		Present		Experiment		Calculated	
$j={}_n\{v\}_m^A$	a_j	E	Γ	E	Γ	E	Γ
${}_2\{0\}_2^+$	2.000	−0.124 242	6.85×10^{-4}			−0.124 328	1.16×10^{-3} [a]
${}_2\{0\}_3^-$	−3.708	−0.126 014	1.06×10^{-6}			−0.126 043 [a]	
${}_3\{0\}_3^+$	−5.220	−0.062 695	1.23×10^{-3}	−0.062 691 [b]	1.23×10^{-3} [b]	−0.062 713 [a]	1.26×10^{-3} [a]
${}_3\{0\}_4^-$	−14.897	−0.058 866	1.48×10^{-5}			−0.058 572 [a]	9×10^{-6} [a]
${}_3\{0\}_4^+$	−5.220	−0.055 832	4.26×10^{-5}	−0.055 731 [d]	5.88×10^{-5} [d]	−0.055 903 [a]	6.65×10^{-5} [a]
${}_4\{0\}_4^+$	−18.458	−0.037 181	1.04×10^{-3}	−0.037 139 [b]	9.37×10^{-4} [b]	−0.037 165 [e]	1.01×10^{-3} [e]
${}_4\{0\}_5^-$	−32.049	−0.034 388	2.67×10^{-5}			−0.034 289 [a]	1.80×10^{-5} [a]

${}_2\{0\}_2^+$	2.000	−0.124 328	1.16×10^{-3} [a]				
${}_2\{0\}_3^-$	−3.708	−0.126 043 [a]					
${}_3\{0\}_3^+$	−5.220	−0.062 713 [a]	1.26×10^{-3} [a]	−0.062 716 [c]	1.20×10^{-3} [c]	−0.062 695	1.23×10^{-3}
${}_3\{0\}_4^-$	−14.897	−0.058 572 [a]	9×10^{-6} [a]	−0.058 571 [c]	8.95×10^{-6} [c]	−0.058 866	1.48×10^{-5}
${}_3\{0\}_4^+$	−5.220	−0.055 903 [a]	6.65×10^{-5} [a]	−0.055 902 [c]	6.85×10^{-5} [c]	−0.055 832	4.26×10^{-5}
${}_4\{0\}_4^+$	−18.458	−0.037 165 [e]	1.01×10^{-3} [e]	−0.037 131 [a]	1.25×10^{-3} [a]	−0.037 181	1.04×10^{-3}
${}_4\{0\}_5^-$	−32.049	−0.034 289 [a]	1.80×10^{-5} [a]			−0.034 388	2.67×10^{-5}

[a] Reference [19].
[b] Reference [40].
[c] Reference [41].
[d] Reference [2].
[e] Reference [15].

extends for some distance above threshold, so that near $E \approx 11.1$ eV the $n=2$ production is roughly three times as likely as is the population of ground-state H atoms. As will be shown below, the populations of the $n=1$ and 2 states become comparable at higher energies.

Partial cross sections for the production of H atoms in $n=1$, 2, and 3 states are shown in Fig. 5(b) for the energy range near the $n=3$ threshold. This plot aids considerably in the interpretation of decay mechanisms. Consider first that the resonances affect the otherwise smooth background of ground-state production as a series of dips—or window resonances with small asymmetries. The dips do not, however, reduce the cross section to zero. This suggests that the $n=3$ resonances decay primarily to $n=2$ states; this will be put on a more quantitative footing in the discussion of the delay-time matrix. Above the $H(n=3)$ threshold, the $H(n=1)$ and $H(n=2)$ continua are, however, populated with equal efficiency. Note, furthermore, the beautifully asymmetric profiles of the resonances seen in the partial cross section for production of $H(n=2)$. The near vanishing of these resonances near their minima indicates the existence of a single dominant continuum for their decay.

The situation changes markedly for the resonances near the $n=4$ threshold, shown in Fig. 5(c). Note once again the nearly equal background values of the $n=1$ and 2 partial cross sections and the smooth joining of the $H(n=1)$ and $H(n=2)$ production cross sections through the range of energies covered in Figs. 5(a)–5(c). The partial cross section for production of $n=3$ fragments is roughly $\frac{1}{3}$ of either $n=1$ or 2, and all resonances have "window" resonance profiles in the $n=3$ decay channel. In opposition, the $n=2$ partial cross sections show resonant "spikes" with small asymmetries.

The large value of the $H(n=2)$ production cross section compared with the production of the $n=3$ excited state of hydrogen *appears* to contradict earlier predictions [5,6,14,25] that the main decay continuum for the autodetachment of the doubly excited resonant states is the nearest available one. We show below, however, that there exists no inconsistency with these predictions for the resonant decay.

In Fig. 6(a), the energy profile of the largest eigenvalue of the delay-time matrix, $q_{\max}(E)$ in Eq. (10), is shown. The energy range covers the lowest members of the + and − series in the $n=4$ manifold, namely the ${}_4\{0\}_4^+$ and ${}_4\{0\}_5^-$ resonances. There are two prominent peaks, described completely by the Lorentzian profile in Eq. (10), as isolated resonances with width $\Gamma = 4/q_{\max}|(E=E_0)$. In Fig. 6(b) we show the absolute square of the two largest components of the corresponding delay-time eigenvector as a function of energy. These components belong to the $j = {}_2\{0\}^+$ and ${}_3\{0\}^+$ detachment channels. It is readily verified that the ${}_4\{0\}_4^+$ resonance decays 73% of the time to the ${}_3\{0\}^+$ channel and 18% to the ${}_2\{0\}^+$ channel at the position of the resonance, −0.037 181 a.u. Hence the decay pathway ${}_4\{0\}^+ \rightarrow {}_3\{0\}^+$ is favored 4 to 1 over the mode ${}_4\{0\}^+ \rightarrow {}_2\{0\}^+$. A similar situation occurs for the decay of ${}_4\{0\}_5^-$ resonance with a probability of 0.96 to the ${}_3\{0\}^-$ channel.

In Fig. 7(a) the partial cross sections for the production of the ${}_3\{0\}^+$ and ${}_3\{0\}^-$ channels are shown in the energy range near the $H(n=4)$ threshold. Two prominant features are present. The first is the well-known general dominance of + channels over the − channels [10,27]; the ${}_3\{0\}^+$ continuum is excited with more than an order of magnitude probability than the ${}_3\{0\}^-$ continuum. More importantly, the vanishing of the cross section at the position of the ${}_4\{0\}_m^+$, with $m=4,5,6\ldots$, resonance series emphasizes once more that the main decay mechanism takes place via their coupling to the ${}_3\{0\}^+$ continuum.

A similar analysis of the delay-time matrix shows that the probability for the decay of the ${}_3\{0\}_3^+$ resonance to the ${}_2\{0\}^+$ photodetachment channel is 0.89 and less than 0.05 to each of the remaining detachment channels. Figure 7(b) shows likewise the vanishing of the cross section for the excitation of the ${}_2\{0\}^+$ continuum at the positions of the ${}_3\{0\}_m^+$ resonance series, as in Fig. 7(a). The ${}_3\{0\}_4^-$ resonance also decays primarily to the ${}_2\{0\}^-$ channel with 94% efficiency. Moreover, we found that the ${}_2\{0\}_2^+$

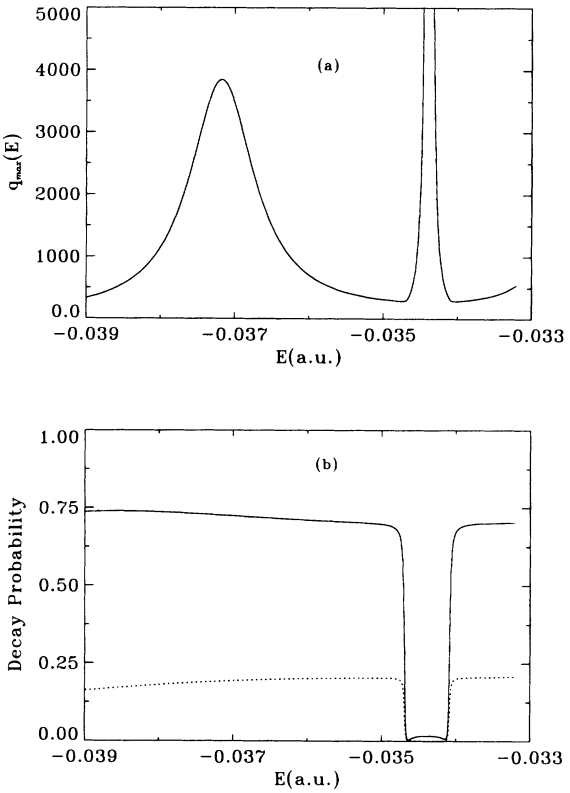

FIG. 6. The parameters of the delay-time matrix $\underline{Q}(E)$ near the $H(n=4)$ threshold; (a) the energy profile of the largest eigenvalue of the delay-time matrix showing the Lorentzian Breit-Wigner shape; (b) the two largest absolute square eigenvector components corresponding to $q_{\max}(E)$ as a function of energy. The ${}_4\{0\}_4^+$ and ${}_4\{0\}_5^-$ resonance positions are, respectively, at −0.037 181 and −0.034 388 a.u. The results of (b) verify that the ${}_4\{0\}_4^+$ resonance is four times more likely to decay via nonradiative autodetachment to the ${}_3\{0\}^+$ channel than to the ${}_2\{0\}^+$ channel. Note also the negligible excitation of the ${}_3\{0\}^+$ and ${}_3\{1\}^+$ continua at the position of the ${}_4\{0\}_5^-$ resonance.

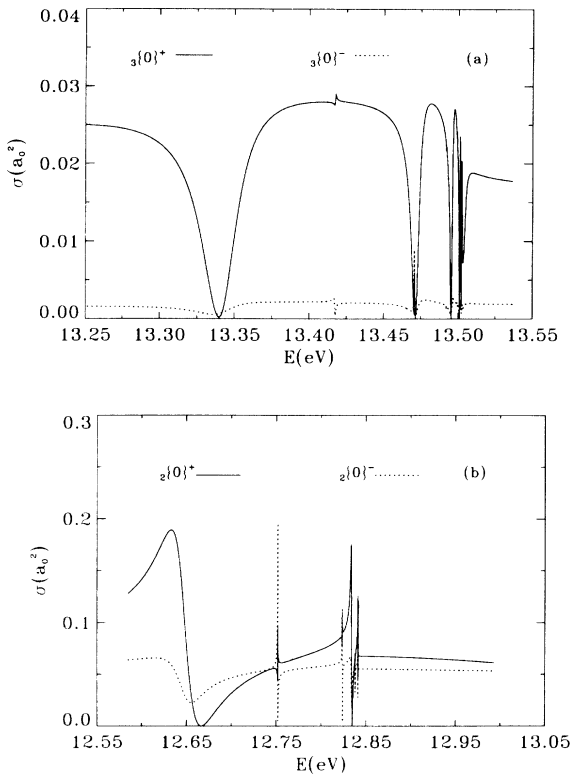

FIG. 7. Partial cross sections for populating the individual photodetachment channels ${}_n\{v\}^A = {}_n\{0\}^A$; (a) the rate of excitation of the ${}_3\{0\}^+$ channel is an order of magnitude larger than the rate for exciting the ${}_3\{0\}^-$ channel at photon energies near the $n=4$ state of hydrogen; (b) similar plot as in (a) for the channels ${}_2\{0\}^+$ and ${}_2\{0\}^-$ near the H($n=3$) threshold. Note the vanishing of the cross sections at the positions of the ${}_n\{0\}^+_m$ resonances in the ${}_n\{0\}^+$ channels.

shape resonance [see Fig. 5(a)] tunnels most effectively to its parent continuum, namely the ${}_2\{0\}^+$ channel, with a probability of 0.89. The electrons remain trapped in this shape resonance for approximately 35 fs.

What the study of the delay-time matrix and the partial cross sections have revealed are that (a) the partial cross sections provide us with information on the continuum population of the hydrogenic states via direct "vertical" electric dipole transitions, and (b) the delay-time matrix $\underline{Q}$ appears to be the variable for study of the excitation and decay of such quasistable states. The resonant excitation of the highly excited states proceeds according to predictions of Ref. [5] via nonadiabatic coupling through avoided crossings of diabatic potential curves. These nonadiabatic transitions approximately conserve the v and A quantum numbers, as expected from Refs. [5] and [24].

IV. SUMMARY

In this work we present an extensive analysis of the H^- excited states using the eigenchannel R-matrix method. The agreement of the total cross sections with the observed spectra near the energies below the H($n=2$) and H($n=3$) thresholds is exceptionally good. The partial cross section for the production of the H($n=2$) excited states for incident photon energies near the H($n=4$) threshold also shows nice accord with the very recent observation of this spectrum [40]. Comparisons with the energy positions and widths of other calculations are rather satisfying.

We show in a quantitative manner the autodecay mechanisms for the doubly excited states of H^- and give probabilities for such decays. Our study based on Smith's derivation of the delay-time matrix establishes quite convincingly that the ${}_n\{0\}^+_m$ resonances decay most readily to the ${}_{n-1}\{0\}^+$ continuum, i.e., the nonradiative decay mode is via coupling to the nearest energetically available detachment channel with the same v and A quantum numbers.

The partial cross sections for the production of the hydrogen atom in the ground and excited states join on as a smooth background in the whole range of energies studied. At high energies, the rate of production of H($n=1$) and H($n>1$) states appears to be roughly equal and is interpreted in terms of continuum excitation via direct dipole transition from the H^- ground state. High-lying resonant states can, however, be excited only via nonadiabatic transitions through the avoided crossings shown in Fig. 1 and discussed in Refs. [5] and [24].

ACKNOWLEDGMENTS

This work was partially supported by the U.S. Department of Energy, Division of Chemical Sciences, Office of Basic Energy Sciences, Office of Energy Research. M.J.C. was supported by a JILA Postdoctoral Fellowship during the early stages of this project. The authors wish to thank M. Halka and H. Bryant for discussions and providing data prior to publication, and also George Victor and Ravi Rau for a reading of this manuscript.

[1] H. C. Bryant, B. D. Dieterie, J. Donahue, H. Sharifian, H. Tootoonchi, D. M. Wolfe, P. A. M. Gram, and M. A. Yates-Williams, Phys. Rev. Lett. **38**, 228 (1977).

[2] M. E. Hamm, R. W. Hamm, J. Donahue, P. A. M. Gram, J. C. Pratt, M. A. Yates, D. R. Bolton, D. A. Clarke, H. C. Bryant, C. A. Frost, and W. W. Smith, Phys. Rev. Lett. **43**, 1715 (1979).

[3] P. G. Harris, H. C. Bryant, A. H. Mohagheghi, R. A. Reeder, H. Sharifian, C. Y. Tang, H. Tootoonchi, J. B. Donahue, C. R. Quick, D. C. Rislove, W. W. Smith, and J. E. Steward, Phys. Rev. Lett. **65**, 309 (1990).

[4] P. G. Harris *et al.*, Phys. Rev. A **42**, 6443 (1990).

[5] H. R. Sadeghpour and C. H. Greene, Phys. Rev. Lett. **65**, 303 (1990).

[6] D. R. Herrick, Phys. Rev. A **12**, 413 (1975).

[7] D. R. Herrick, Adv. Chem. Phys. **52**, 1 (1983).

[8] A. R. P. Rau, At. Unusual Situat. **143**, 383 (1985).

[9] J. H. Macek, J. Phys. B **1**, 831 (1968).

[10] C. D. Lin, Phys. Rev. Lett. **30**, 1150 (1975); Phys. Rev. A **14**, 30 (1976).

[11] U. Fano, Rep. Prog. Phys., **46**, 97 (1983); C. D. Lin, Adv. At. Mol. Phys. **22**, 77 (1986).
[12] N. Koyama, H. Fukuda, T. Motoyama, and M. Matsuzawa, J. Phys. B **19**, L331 (1986); N. Koyama, A. Takafuji, and M. Matsuzawa, *ibid.* **22**, 553 (1989).
[13] J. M. Feagin and J. S. Briggs, Phys. Rev. Lett. **57**, 984 (1986).
[14] J. M. Rost and J. S. Briggs, J. Phys. B **21**, L233 (1988); **23**, L339 (1990).
[15] Y. K. Ho and J. Callaway, Phys. Rev. A **34**, 130 (1986).
[16] Y. K. Ho, Phys. Rep. **99**, 1 (1983).
[17] C. A. Nicolaides and Y. Komninos, Phys. Rev. A **35**, 999 (1987).
[18] J. T. Broad and W. P. Reinhardt, Phys. Rev. A **14**, 2159 (1976).
[19] A. Pathak, A. E. Kingston, and K. A. Berrington, J. Phys. B **21**, 2939 (1988).
[20] (a) C. H. Greene, J. Phys. B **13**, L39 (1980); (b) H. A. Hyman, V. L. Jacobs, and P. G. Burke, *ibid.* **5**, 2282 (1972); (c) C. R. Liu, N. Y. Du, and A. F. Starace, Phys. Rev. A **43**, 5891 (1991).
[21] S. M. Burkov, N. A. Letyaev, and S. I. Strakhova, Phys. Lett. A **150**, 31 (1990).
[22] A. R. P. Rau, Phys. Rep. **110**, 369 (1984).
[23] F. T. Smith, Phys. Rev. **118**, 349 (1960).
[24] H. R. Sadeghpour, Phys. Rev. A **43**, 5821 (1991).
[25] S. Watanabe and C. D. Lin, Phys. Rev. A **34**, 823 (1986).
[26] C. D. Lin, Phys. Rev. Lett. **51**, 1348 (1983).
[27] J. W. Cooper, U. Fano, and F. Pratts, Phys. Rev. Lett. **10**, 518 (1963).
[28] P. G. Burke and W. D. Robb, Adv. At. Mol. Phys. **11**, 143 (1974).
[29] U. Fano and C. M. Lee, Phys. Rev. Lett. **31**, 1573 (1973).
[30] C. H. Greene and P. O'Mahony, Phys. Rev. A **31**, 250 (1985); C. H. Greene and L. Kim, *ibid.* **36**, 2706 (1987).
[31] C. H. Greene, in *Fundamental Processes of Atomic Physics,* edited by J. S. Briggs, H. Kleinpoppen, and H. O. Lutz (Plenum, New York, 1988).
[32] M. J. Seaton, Proc. Phys. Soc. **77**, 174 (1961).
[33] M. Gailitis and R. Damburg, Proc. Phys. Soc. London **82**, 192 (1963).
[34] C. H. Greene and Ch. Jungen, Adv. At. Mol. Phys. **21**, 51 (1985).
[35] U. Fano and A. R. P. Rau, *Atomic Collisions and Spectra* (Academic, New York, 1986).
[36] C. Greene, U. Fano, and G. Strinati, Phys. Rev. A **19**, 1485 (1979).
[37] M. J. Seaton, Proc. Phys. Soc. London **88**, 801 (1966).
[38] F. H. Read, J. Phys. B **10**, 449 (1977); A. R. P. Rau, *ibid.* **16**, L699 (1983).
[39] M. Cavagnero, Z. Zhen, and J. H. Macek, Phys. Rev. A **41**, 1225 (1990).
[40] M. Halka, H. C. Bryant, E. P. Mackerrow, W. Miller, A. H. Mohagheghi, C. Y. Tang, S. Cohen, J. B. Donahue, A. Hsu, C. R. Quick, J. Tiee, and K. Rosza, Phys. Rev. A **44**, 6127 (1991).
[41] J. Callaway, Phys. Lett. **75A**, 43 (1979).